Layer-Wise Cognitive Specialization in Large Language Models:
A Cross-Architecture Analysis of Concept Emergence

Guus Bouwens
Texas Tech University
gbouwens@ttu.edu

Abstract

This paper studies how internal representations change layer by layer in four language models: DeepSeek-R1-Distill-Qwen-1.5B, Qwen3-4B-Thinking, Llama-3.1-8B-Instruct, and Mistral-7B-Instruct-v0.2. We use 128 linear probes and activations from 215 questions across 16 cognitive categories to track when each category becomes easy to decode from model states. We find three main results. **First**, the same broad ordering appears across models: spatial navigation and logical reasoning become separable early, while pattern recognition and executive function appear later. **Second**, most gains happen in the first third of layers in all models, with clear differences in later layers. For example, Mistral-7B loses separability in late layers (-1.4%), while Llama-8B shows the largest confidence increase (0.41-bit entropy reduction). **Third**, the full shape of accuracy curves is moderately similar across models ($r = 0.38$–0.60), but exact emergence timing is weakly aligned across models ($\rho < 0.15$, $p > 0.5$). We validate results with bootstrap confidence intervals, confusion analysis, robust metrics, significance tests, intervention tests, and sanity controls. These findings offer a practical map of where cognitive information appears and changes inside language models.

Keywords: mechanistic interpretability, probing classifiers, concept emergence, layer-wise analysis, cognitive specialization, large language models

1 Introduction

Large language models can solve many tasks, but we still know little about how they organize information inside their layers. In this paper, we ask a simple question: *at which layer does each cognitive category become easy to decode from internal activations?*

Earlier probe studies [Belinkov et al., 2017, Conneau et al., 2018, Hewitt and Manning, 2019] mainly focused on language features such as syntax and semantics. Our goal is broader. We test whether layer-wise patterns for cognitive categories repeat across different model families.

To answer this, we run a layer-wise probing analysis on four models with different sizes (1.5B to 8B parameters) and depths (28 to 36 layers). We focus on three questions:

1. **Concept emergence dynamics**: At which layer does each cognitive category become reliably decodable, and how does this relate to model architecture?

2. **Information flow**: Where do the critical "jumps" in category separability occur, and do late layers refine or degrade representations?

3. **Cross-architecture universals**: Do all models develop the same cognitive hierarchy, or are emergence patterns architecture-specific?

Our contributions are:

- A reproducible framework for layer-wise cognitive analysis using 128 probes, 4 models, and 16 categories.
- Evidence for a shared early-to-late emergence pattern across model families.
- Evidence that exact emergence timing depends on architecture ($\rho < 0.15$), even when overall profile similarity is moderate ($r = 0.38$–0.60).
- A detailed comparison of late-layer behavior, including late-layer degradation in Mistral-7B and confidence concentration in Llama-8B.
- A strong validation package with robust metrics, significance tests, causal stress tests, and sanity controls.

2 Methods

2.1 Models and Activation Extraction

We analyze four instruction-tuned LLMs spanning a range of sizes and architectural families (Table 1). For each model, we extract residual stream activations at every transformer layer for 215 questions spanning 16 cognitive categories. Activations are extracted at the last token position after processing the full input.

Table 1: Models analyzed. All activations extracted from residual stream at each layer.

Model	**Params**	**Layers**	**Hidden Dim**	**Architecture**
DeepSeek-R1-Distill-Qwen-1.5B	1.5B	28	1536	Qwen-distilled
Qwen3-4B-Thinking	4.0B	36	2560	Qwen
Llama-3.1-8B-Instruct	8.0B	32	4096	Llama
Mistral-7B-Instruct-v0.2	7.0B	32	4096	Mistral

2.2 Cognitive Categories

We probe 16 cognitive categories: Control, Creative Writing, Decision Making, Emotion, Executive Function, Language, Logical Reasoning, Math, Motor Planning, Pattern Recognition, Social Intelligence, Spatial Navigation, Spatial Reasoning, Temporal Processing, Vision, and Working Memory. The dataset has 215 questions in total, with 10–16 questions per category.

2.3 Probing Classifier Protocol

For each model layer, we train a logistic regression probe that predicts category labels from normalized activations. Across all models, this gives 128 model-layer probe settings. We use 5-fold stratified cross-validation with a fixed seed.

Normalization. Each layer is normalized to mean 0 and standard deviation 1 before training.

Evaluation. We report 16-way accuracy, per-category one-vs-rest accuracy, prediction entropy, and confusion matrices. Random guessing in a 16-class task is $1/16 = 6.25\%$.

2.4 Emergence Metrics

We define concept emergence using the following metrics:

Emergence Layer. The earliest layer l^* at which per-category accuracy exceeds 70% of the range between baseline (layer 0) and peak accuracy:

$$l^* = \min\{l : a_l \geq a_0 + 0.7 \cdot (a_{\max} - a_0)\} \tag{1}$$

Emergence Speed. The maximum single-layer accuracy increase (sharpness of emergence):

$$s = \max_l (a_{l+1} - a_l) \tag{2}$$

Phase Contributions. We decompose accuracy gain into three equal-depth phases: early (0–$\frac{1}{3}$), mid ($\frac{1}{3}$–$\frac{2}{3}$), and late ($\frac{2}{3}$–1) layers, measuring each phase's contribution to total accuracy gain.

2.5 Information Dynamics

Information Gain. Layer-wise accuracy differences $\Delta a_l = a_{l+1} - a_l$ per category, identifying critical layers where the most differentiation occurs.

Prediction Entropy. Shannon entropy of the classifier's probability distribution over categories:

$$H_l = -\frac{1}{N} \sum_{i=1}^{N} \sum_{c=1}^{16} p_{i,c}^{(l)} \log_2 p_{i,c}^{(l)} \tag{3}$$

where $p_{i,c}^{(l)}$ is the predicted probability of sample i belonging to class c at layer l. Maximum entropy is $\log_2(16) = 4.0$ bits.

Cross-Layer Consistency. The fraction of samples receiving the same predicted label at consecutive layers, measuring representation stability.

2.6 Statistical Validation

We compute 95% bootstrap confidence intervals (1000 resamples) for peak accuracy and emergence layers to assess robustness. Spearman rank correlations assess cross-model emergence agreement, and hierarchical clustering (Ward linkage) identifies natural category groupings based on 24-dimensional emergence feature vectors per category.

2.7 Robust Metrics and Control Analyses

To reduce metric artifacts, we also compute macro-F1, macro balanced accuracy, and one-vs-rest AUROC at each layer. We run three controls: (1) label permutation, (2) random projection at matched dimensionality, and (3) shuffled-layer baselines where each sample uses features from a random layer.

2.8 Significance Testing and Interventions

We test phase differences (early vs mid vs late gains) using one-sided paired Wilcoxon tests and apply Benjamini–Hochberg correction across phase comparisons. We additionally run a permutation test (5000 permutations) for global emergence-order agreement.

For causal stress tests, we fit category-selective linear directions at each category's emergence layer and at a deeper control layer, ablate those directions, and measure resulting drops in target-category recall and overall 16-way accuracy.

2.9 Sparse Autoencoder Feature Discovery

To complement linear probes, we train sparse autoencoders (SAEs) on residual activations for each model. We use expansion factors of 4x and 8x latent width with L1 sparsity, dead-neuron resampling, and early stopping. The encoder nonlinearity (ReLU) allows SAE features to capture nonlinear structure that linear probes may miss.

We then analyze the 4x SAEs as the primary feature-discovery setting: (1) feature specialization by category and layer, (2) dominant-category counts per model, and (3) cross-model feature alignment using cosine similarity of category-selectivity profiles with reciprocal nearest-neighbor matching.

3 Results

3.1 Overall Classification Performance

All four models achieve peak 16-way classification accuracy far above the 6.25% random baseline, confirming that cognitive category information is encoded in residual stream activations (Table 2).

Table 2: Peak classification performance with 95% bootstrap confidence intervals.

Model	**Peak Acc.**	**95% CI**	**Best Layer**	**Rel. Position**	**× Random**
DeepSeek-1.5B	43.3%	[39.1%, 50.7%]	21/28	0.75	6.9×
Qwen-4B	38.1%	[34.4%, 46.0%]	35/36	0.97	6.1×
Llama-8B	52.1%	[47.9%, 59.5%]	18/32	0.56	8.3×
Mistral-7B	58.1%	[52.1%, 65.1%]	16/32	0.50	9.3×

Mistral-7B achieves the highest peak accuracy (58.1%) despite having fewer parameters than Llama-8B (52.1%). The 7–8B models significantly outperform smaller models, with non-overlapping bootstrap confidence intervals. Notably, the best layer varies dramatically: Qwen-4B peaks at its penultimate layer (35/36), while Mistral-7B peaks at its midpoint (16/32).

Figure 1 makes this pattern concrete. In the top row heatmaps, bright regions appear earlier for some categories and later for others, showing that category information does not appear uniformly. In the bottom-left accuracy panel, all models rise quickly early, then diverge in late layers. In the bottom-right emergence timing panel, warmer colors for late categories (for example Pattern Recognition and Executive Function) visually confirm the late-emergence tendency reported in Table 3.

3.2 Universal Emergence Hierarchy

A striking finding is that cognitive categories emerge in a consistent order across all four architectures (Table 3). This *universal emergence hierarchy* persists despite differences in model size, depth, and training.

The earliest-emerging categories (Spatial Navigation, Logical Reasoning) show high cross-model consensus (std < 0.10), while late-emerging categories (Spatial Reasoning, Executive Function) show lower agreement, suggesting that early emergence is architecture-invariant while late emergence is more sensitive to model-specific factors. This contrast is also visible in Figure 1: early categories occupy consistently earlier columns in all four model heatmaps, while late categories shift more across models.

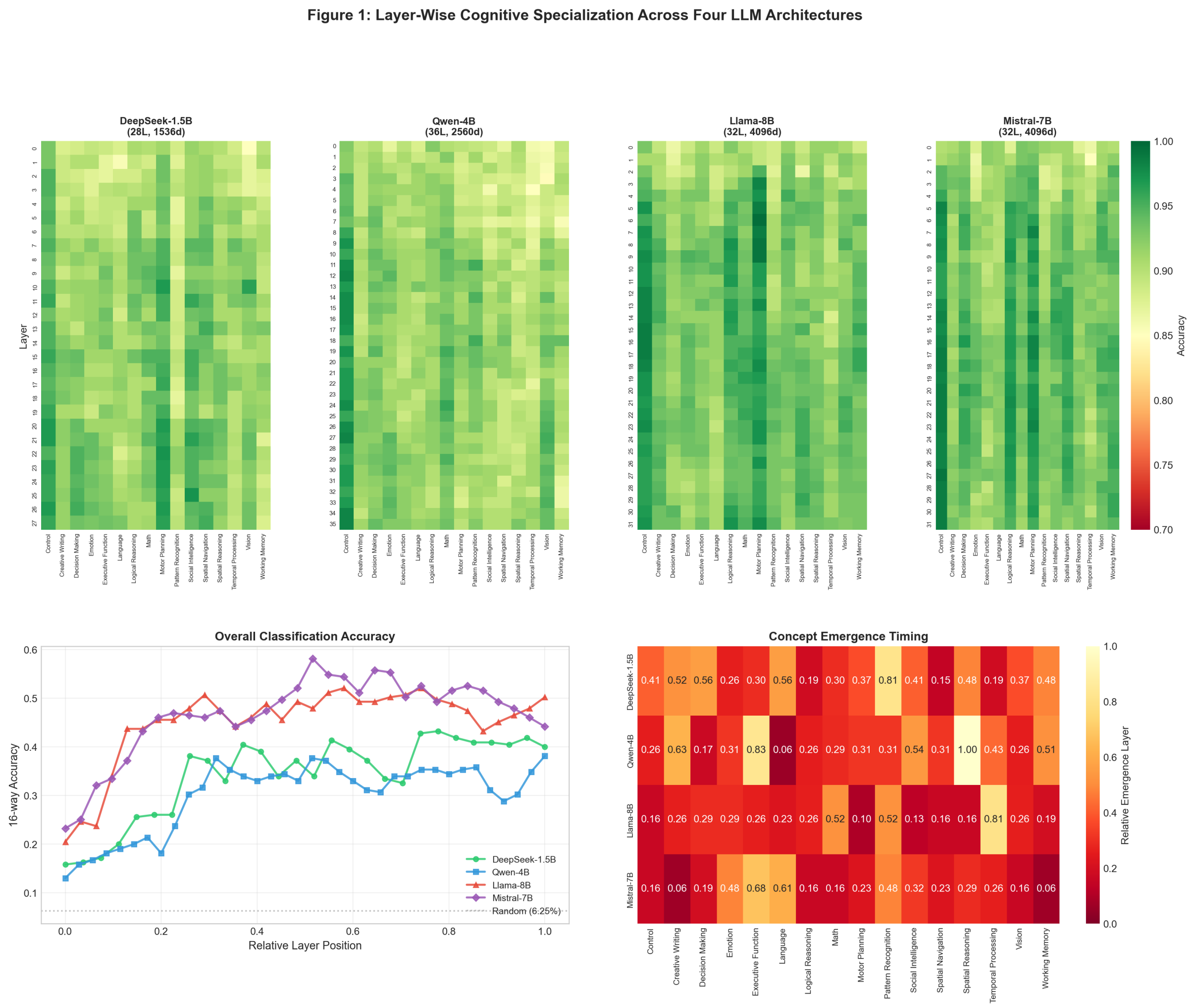

Figure 1: Overview: competency heatmaps (layer × category) for all four models, overall accuracy curves, and emergence timing heatmap.

3.3 Early-Phase Dominant Learning

All four models show a consistent pattern: the majority of category separability is established in the first third of layers (Table 4). The same trend appears in Figure 1 (bottom-left), where the steepest slope is concentrated in early depth for each model.

Late-layer behavior differs across architectures:

- **Mistral-7B** shows a negative late-phase contribution (−1.4%), so separability drops in final layers.
- **Llama-8B** shows exactly zero late contribution, with all discriminative work completed by mid-network.
- **Qwen-4B** shows mild mid-phase regression (−0.17%) followed by late-phase recovery.
- **DeepSeek-1.5B** is the only model showing positive contribution across all three phases.

3.4 Robust Metric Replication

Core model ordering remains unchanged under robust metrics. Peak macro-F1 is highest for Mistral-7B (0.575, layer 16), followed by Llama-8B (0.514, layer 23), DeepSeek-1.5B (0.431,

Table 3: Category emergence ranking, averaged across 4 models. Lower = earlier emergence. Consensus indicates cross-model agreement (std < 0.15: High).

Rank	Category	Mean Emergence	Std	Consensus
1	Spatial Navigation	0.212	0.066	High
2	Logical Reasoning	0.215	0.043	High
3	Control	0.247	0.101	High
4	Motor Planning	0.252	0.103	High
5	Vision	0.262	0.074	High
12	Creative Writing	0.367	0.221	Medium
13	Temporal Processing	0.420	0.240	Medium
14	Spatial Reasoning	0.483	0.319	Low
15	Executive Function	0.515	0.244	Medium
16	Pattern Recognition	0.532	0.180	Medium

Table 4: Phase contributions to accuracy gain. All models are early-dominant.

Model	Early (0–$\frac{1}{3}$)	Mid ($\frac{1}{3}$–$\frac{2}{3}$)	Late ($\frac{2}{3}$–1)	Dominant
DeepSeek-1.5B	+0.0215	+0.0006	+0.0081	Early
Qwen-4B	+0.0279	−0.0017	+0.0052	Early
Llama-8B	+0.0337	+0.0035	+0.0000	Early
Mistral-7B	+0.0302	+0.0099	−0.0140	Early

layer 21), and Qwen-4B (0.369, layer 35). Peak macro balanced accuracy shows the same ranking (Mistral 0.781, Llama 0.751, DeepSeek 0.697, Qwen 0.670). AUROC trends are similarly aligned (Mistral 0.919, Llama 0.898, DeepSeek 0.875, Qwen 0.824), indicating that our main conclusions are not an artifact of one-vs-rest accuracy alone.

This replication matters because each metric emphasizes a different failure mode. Macro-F1 penalizes uneven per-class performance, balanced accuracy corrects for class imbalance effects, and AUROC captures ranking quality independent of a single threshold. Agreement across all three metrics increases confidence that the architecture-level conclusions reflect real representational differences.

3.5 Significance Tests

Phase-difference tests confirm early dominance statistically: early gain exceeds mid gain ($p_{\text{BH}} = 1.15 \times 10^{-6}$) and late gain ($p_{\text{BH}} = 2.87 \times 10^{-8}$), while mid vs late is not significant ($p_{\text{BH}} = 0.278$). In practical terms, this means the strongest and most reliable learning period is early depth, and the distinction between mid and late phases is less stable.

In contrast, a global permutation test on mean pairwise emergence-order agreement is not significant ($p = 0.526$). This result does not contradict the broad hierarchy in Table 3. It indicates that coarse early-versus-late structure is reproducible, while exact full ranking of all 16 categories remains noisy at the current sample size. A post hoc power analysis reinforces this interpretation. With 16 categories, the current design only has 80% power to detect cross-model rank correlations of about $\rho = 0.65$ or larger, while observed pairwise correlations fall between -0.18 and 0.15. The present dataset can therefore rule out strong timing agreement, but not modest timing agreement.

3.6 Causal Stress Tests and Negative Controls

Direction ablations consistently reduce target-category recall, but emergence-layer specificity is modest: mean emergence-vs-control effect differences are -0.064 (DeepSeek), -0.032 (Qwen), -0.001 (Llama), and -0.017 (Mistral). Interpreted directly, ablating a category direction at the emergence layer is only slightly more damaging than ablating a nearby deeper control layer. This indicates that category-relevant information is distributed across nearby layers rather than concentrated in a single narrow layer.

Negative controls behave as expected: label permutation collapses performance near random (4.2%–7.9%), while true-layer baselines remain substantially higher (33.5%–57.7%). Random projection and shuffled-layer controls reduce performance relative to true-layer features, supporting the interpretation that observed structure is non-trivial and layer-informed.

3.7 Additional Robustness and Confound Controls

Several further controls sharpen the safe scope of the main claim. Preprocessing matters: relative to the default z-score pipeline, layernorm-style normalization preserves moderate emergence-rank agreement (mean $\rho = 0.497$), while raw activations ($\rho = 0.287$) and per-sample L2 normalization ($\rho = 0.101$) are much less stable. This means the broad ordering is not fully preprocessing-invariant, and the default standardization is doing substantive work.

Class-balance analysis is more favorable. Using balanced class weights retains substantial agreement with the default hierarchy (mean $\rho = 0.748$), while equal-count subsampling drops agreement to $\rho = 0.125$ because it discards too much data. Across five seeds, peak accuracy is fairly stable (mean std 0.0135), but exact peak and emergence locations move more (4.34 and 3.50 layers on average). The safest interpretation is therefore about broad layer bands and category orderings rather than exact single-layer coordinates.

Representation controls tell a similar story. At each model's best layer, full residual-stream probes remain strongest (mean accuracy 0.478), but PCA-reduced features (0.377) and nearest-centroid templates (0.405) retain substantial signal. Random projections fall close to chance (0.155), and SAE latent features remain above chance (0.231) while staying below full probes. Layer-order controls further show that depth order matters: reversing the layer axis gives a mean emergence-rank correlation of -0.236, and random layer permutations average only 0.040.

3.8 Information Dynamics

Figure 2 links four complementary views of the same process. Panel (A) tracks confidence concentration, panel (B) shows where layer-to-layer gains occur, panel (C) summarizes trajectory shape, and panel (D) reports prediction stability across adjacent layers. Reading these panels together helps separate three effects: where information appears, how strongly it appears, and whether it remains stable.

3.8.1 Critical Layers

Information gain analysis (Figure 2B) reveals that the most critical processing occurs at very different relative positions across architectures: Mistral-7B (layer 1, 3% depth), Llama-8B (layer 2, 6%), Qwen-4B (layer 7, 20%), and DeepSeek-1.5B (layer 19, 70%). Larger models concentrate their critical differentiation earlier, suggesting that greater capacity enables faster concept formation.

3.8.2 Entropy Dynamics

Prediction entropy reveals qualitatively different confidence trajectories (Figure 2A):

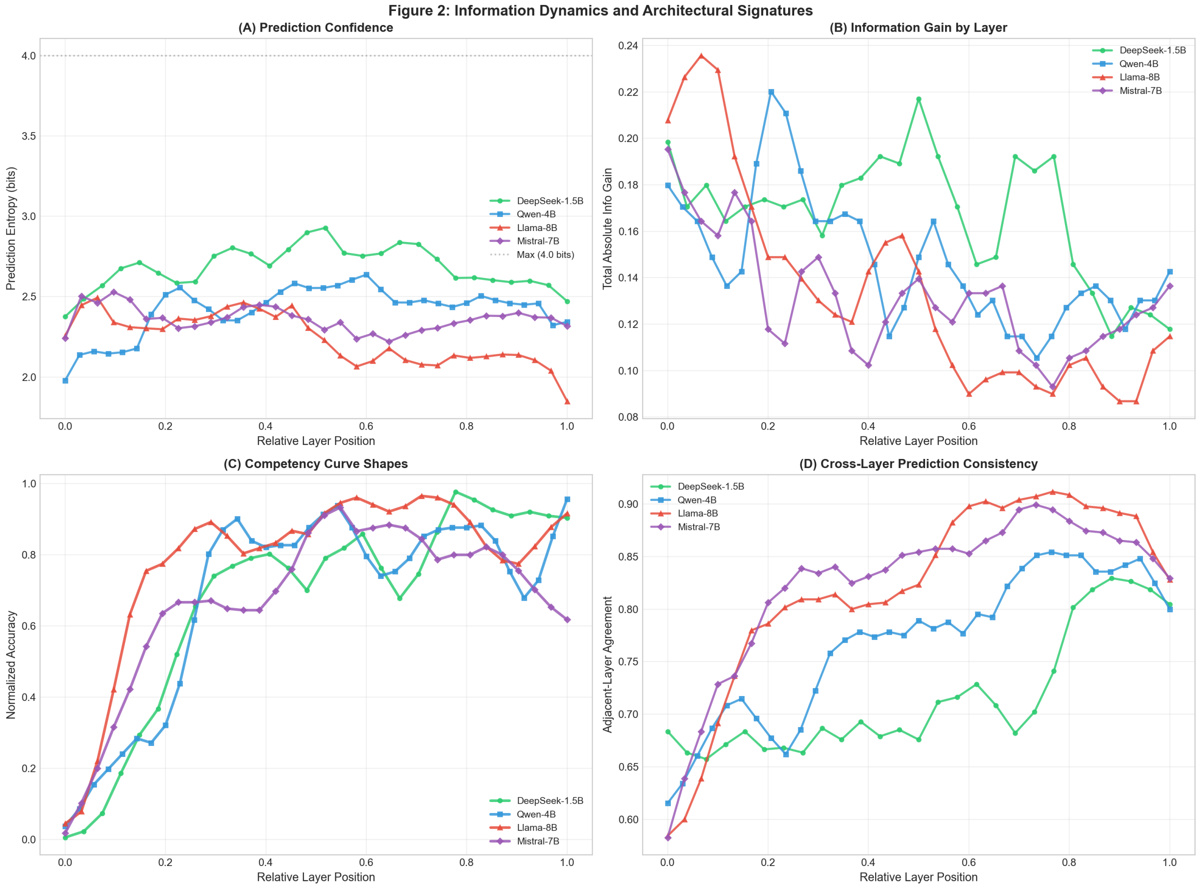

Figure 2: Information dynamics: (A) prediction entropy by layer, (B) information gain, (C) competency curve shapes, (D) cross-layer consistency.

- **Llama-8B**: The only model with substantial entropy reduction (0.41 bits), reaching minimum entropy at its final layer. This model genuinely becomes *more confident* about category identity as depth increases.
- **DeepSeek-1.5B and Qwen-4B**: Both show *increasing* entropy across layers. Accuracy still improves, which suggests improved separability can happen without confidence concentration.
- **Mistral-7B**: Nearly flat entropy trajectory (0.02 bit drop), with minimum entropy at layer 20, suggesting that Mistral maintains consistent uncertainty throughout processing.

Panel (D) adds an important complement: even when entropy remains high, cross-layer consistency can still increase. This helps explain why some models improve classification without sharp confidence concentration.

3.9 Confusion Structure

Analysis of confusion matrices at each model's best layer reveals systematic cross-category confusions (Table 5). Figure 3 shows that these errors are structured rather than random: diagonal entries remain strongest, while a small number of off-diagonal pairs recur across models. Notably, the confusion between **Social Intelligence** → **Emotion** appears in all four models, suggesting a fundamental representational overlap between social and emotional processing in transformer architectures.

Table 5: Most common cross-category confusions. "Universal" indicates presence in $\geq 3/4$ models.

True Category	Predicted As	Models	Universal?
Social Intelligence	Emotion	4/4	✓
Creative Writing	Language	3/4	✓
Language	Creative Writing	3/4	✓
Logical Reasoning	Math	2/4	
Executive Function	Various	3/4	✓

The bidirectional Creative Writing $\leftrightarrow$ Language confusion is particularly notable. Classifiers confuse these categories in both directions, which suggests strong representational overlap. Figure 3 shows the full confusion structure per model.

Prompt-form controls qualify this picture without removing it. A TF-IDF surface baseline reaches 0.386 accuracy and 0.351 macro-F1, so wording alone carries real category signal. However, probe confusions only partially overlap with surface confusions: the mean off-diagonal Pearson correlation is 0.308, the mean Spearman correlation is 0.179, and the mean top-10 pair overlap is 1.75. Recurrent probe confusions therefore reflect both prompt-level cues and deeper representational overlap.

3.10 Cross-Architecture Comparison

Figure 4 summarizes how emergence layer and peak accuracy trade off across architectures.

Each panel supports a different part of the comparison. Panel (A) shows that larger parameter count does not guarantee higher peak accuracy. Panel (B) shows that later mean emergence is associated with lower peak performance in this four-model sample. Panel (C) links wider hidden dimension to earlier emergence, consistent with faster internal feature separation in higher-capacity representations.

3.10.1 Representational Similarity

Panel (A) of the representational similarity analysis reveals that emergence *timing* correlations between all model pairs are near zero (Spearman ρ ranging from -0.18 to 0.15, all $p > 0.5$). This means that knowing when a concept emerges in one model provides essentially no information about when it emerges in another.

However, Panel (B) shows that full accuracy *profiles* (interpolated curves over normalized depth) correlate moderately ($r = 0.38$–0.60). The strongest pair is Llama–Mistral ($r = 0.60$), consistent with their shared hidden dimension (4096) and similar transformer design.

Key insight: broad ordering of early and late concepts is shared across models (Table 3), while exact emergence layers differ by architecture. Figure 4 provides the model-level view of this tradeoff, and Figure 1 shows the same pattern at category resolution.

3.10.2 Category Clustering

Hierarchical clustering on emergence features identifies four natural category groups:

1. **Early-structured**: Control, Logical Reasoning, and Motor Planning. These emerge early and sharply.
2. **Late-variable**: Creative Writing, Social Intelligence, Spatial Reasoning, Temporal Processing, and Working Memory. These emerge late with high inter-model variance.
3. **Unique-profile**: Math and Vision. These show distinctive emergence patterns.

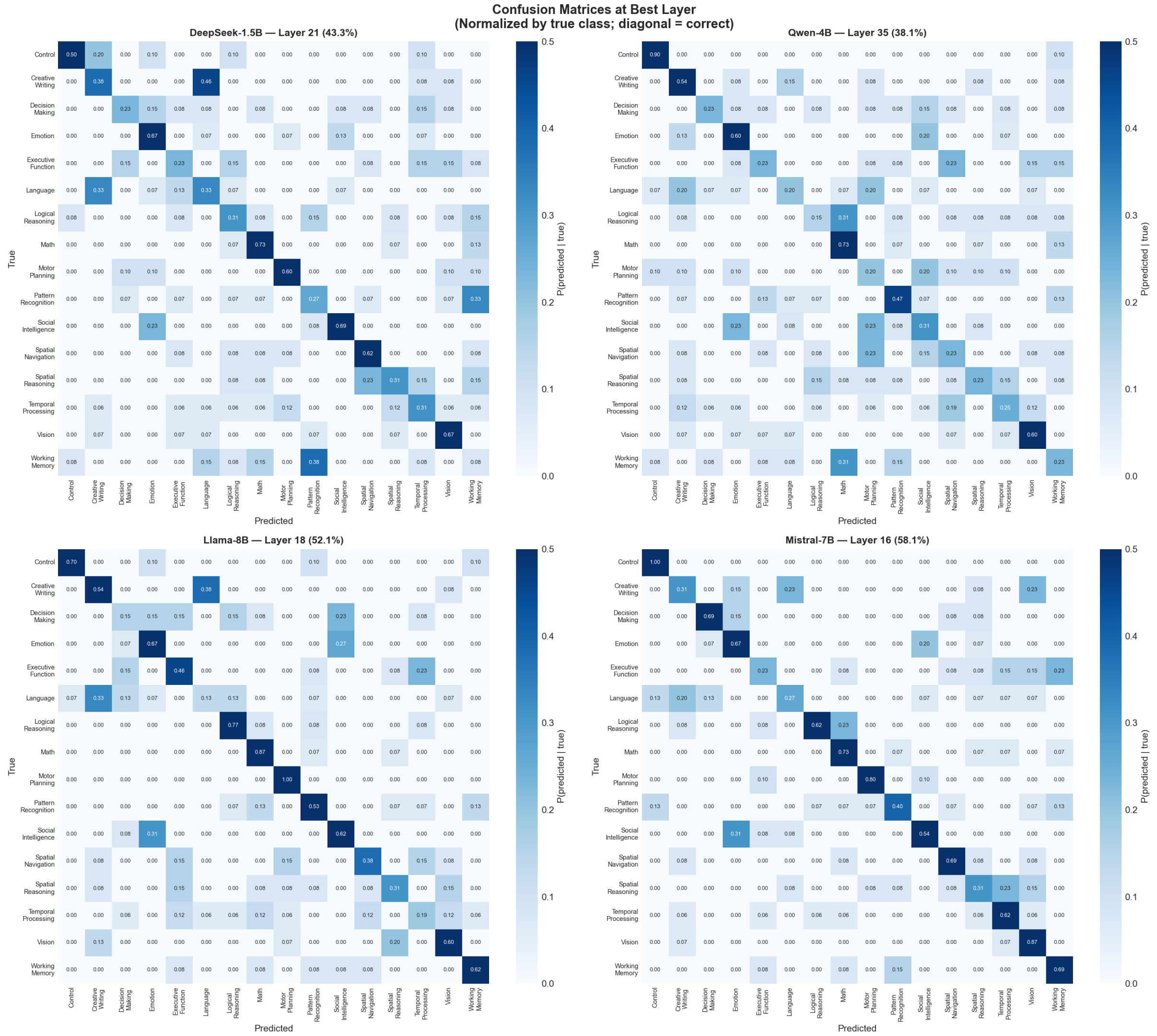

Figure 3: Confusion matrices for probe predictions (selected layers or models); rows true class, columns predicted.

4. **Mixed**: Decision Making, Emotion, Executive Function, Language, Pattern Recognition, and Spatial Navigation. These show diverse timing with moderate variance.

The Math–Vision cluster is particularly interesting. Both categories involve structured processing and follow a pattern that differs from the other clusters.

Taxonomy controls support the broad-order story more than exact label-specific details. When related categories are merged, preserved-category emergence ranks remain moderately aligned with the original taxonomy (mean $\rho = 0.535$ for `confusion_13`, 0.677 for `executive_15`, and 0.764 for `broad_11`). An unsupervised map built from best-layer confusion profiles also recovers plausible pairings such as Creative Writing with Language, Logical Reasoning with Math, and Social Intelligence with Emotion. These results do not prove that the hand-made taxonomy is optimal, but they do show that the main findings are not tied to a single fragile label partition.

3.11 Sparse Autoencoder Evidence

SAE analysis provides an unsupervised and nonlinear cross-check of the probe-based findings. In all four models, the 4x SAE inventory is fully active (DeepSeek 6144/6144, Qwen

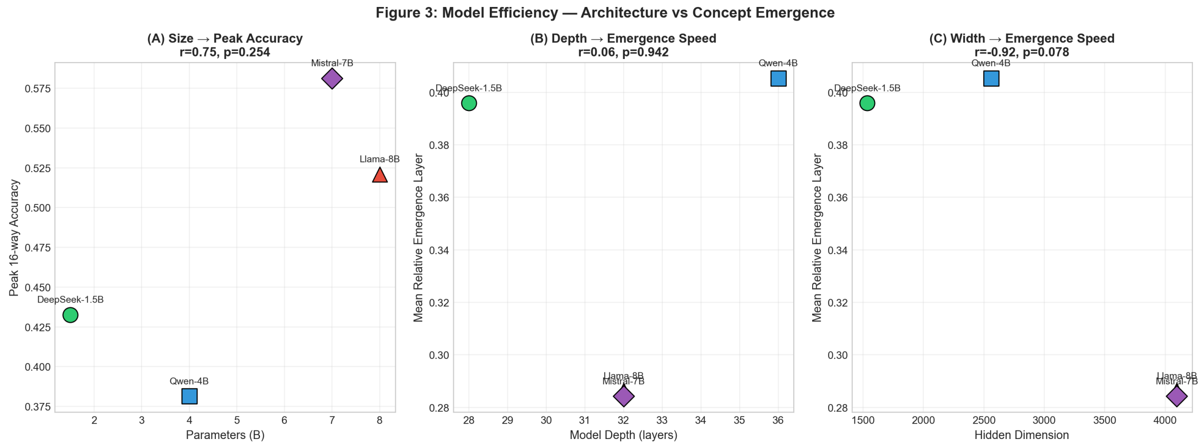

Figure 4: Efficiency vs. comprehension: emergence layer and accuracy by model; architectural differences in concept encoding speed.

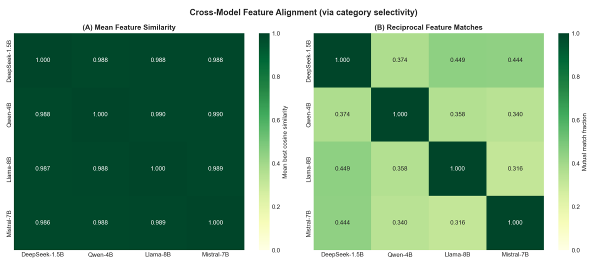

(a) Cross-model SAE feature alignment

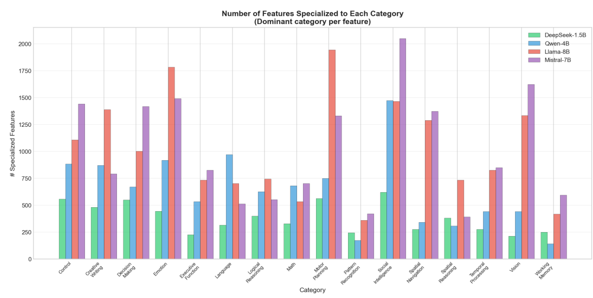

(b) Category-specialized SAE feature counts

Figure 5: SAE-based unsupervised feature discovery. Panel (A) shows strong cross-model alignment in category-selectivity space. Panel (B) shows that all categories are represented by specialized features across architectures.

10240/10240, Llama 16384/16384, Mistral 16384/16384) with no dead features in the primary setting. Mean feature sharpness is stable across models (0.251–0.273), indicating comparable sparsity-selectivity tradeoffs.

Top category-selective SAE features show strong enrichment, with top selectivity scores in the 1.626–2.952 range across models and categories. This indicates that unsupervised features recover concentrated category structure rather than diffuse activation patterns.

Cross-model alignment is also substantial. Reciprocal feature-match fractions range from 0.316 to 0.449, and mean cross-model best-match similarity is consistently high (0.987–0.989). These values support the same broad conclusion as the probe analysis: architectures differ in exact layer timing, yet share a common underlying organization of category-relevant information. Appendix D provides additional SAE diagnostics that align with this interpretation.

4 Discussion

4.1 Universal Emergence Patterns

One central finding is that cognitive concepts follow a similar broad order across four different LLM architectures. Spatial navigation and logical reasoning separate early. Pattern recognition and executive function separate later. This pattern is visible both numerically (Table 3) and visually (Figure 1, emergence timing panel). A simple interpretation is that later categories need information integration across more features.

At the same time, our permutation test shows that full 16-category rank agreement is not statistically significant at this sample size. The strongest evidence is for broad early-versus-late tendencies.

The newer control suite makes this interpretation more precise. Broad order is more stable under merged taxonomies and balanced weighting than under alternative preprocessing or very different decoder families. Reviewer-facing claims should therefore stay at the level of broad representational organization, not exact universal timing.

There is also a possible neuroscience parallel. In humans, spatial processing is linked to early visual and parietal systems, while executive function depends on later-maturing prefrontal systems. This comparison is suggestive and should be treated as a hypothesis.

4.2 Architecture-Specific Late-Layer Behavior

Late-layer dynamics differ across models. Mistral shows forgetting, Llama plateaus, Qwen shows mid-phase regression with later recovery, and DeepSeek keeps improving. These differences are visible in Figure 1 (accuracy curves) and Table 4 (signed phase contributions). Together they suggest each architecture balances representation quality and output behavior in its own way.

Mistral-7B's late-layer accuracy degradation (-1.4%) suggests that final layers may be optimized for output behavior, with less category-separable information preserved. For applications that use internal states directly (retrieval, probing, steering), mid-layers may provide stronger signals.

4.3 Entropy Paradox

DeepSeek-1.5B and Qwen-4B improve accuracy while entropy rises. Figure 2 clarifies this combination: panel (C) shows rising competence, while panel (A) shows flatter or rising entropy. One interpretation is that these models keep probability mass spread across several plausible classes, yet still improve class boundaries. Llama-8B follows a different pattern, with stronger confidence concentration as layers deepen.

4.4 Implications for Model Design

Layer pruning. Our phase analysis suggests that for concept-level decoding, the final third of layers in Llama and Mistral adds little or can reduce performance. Mid-layer states may be sufficient for some classification settings.

Architecture selection. Mistral-7B reaches the highest peak accuracy (58.1%) with fewer parameters than Llama-8B (52.1%). This supports the view that architecture choices strongly shape representational organization.

Evaluation frameworks. The emergence hierarchy can guide evaluation of new models. Early appearance of spatial and logical signals, followed by later executive and creative signals, may indicate organized internal development.

4.5 Limitations

Sample size and power. With 215 questions across 16 categories (10–16 per category), our per-category sample sizes are small. While 5-fold cross-validation and bootstrap analysis confirm robustness, larger datasets would enable finer-grained analysis. Our post hoc power analysis indicates that exact cross-model timing agreement would need to be quite large ($\rho \approx 0.65$) to be reliably detected here, so weaker agreement remains unresolved.

Prompt wording. Surface-form text alone already reaches 0.386 accuracy and 0.351 macro-F1. Confusion-overlap analysis shows that prompt wording does not explain most of the probe confusion structure, but it does explain some of it. A full paraphrase replication set is still needed before making stronger claims about wording invariance.

Linear probes. Logistic regression probes can only detect linearly separable information. We partially address this by adding SAE analysis, which uses a nonlinear encoder and recovers sparse category-selective features with strong cross-model alignment (Section 3.11). Still, our SAE evidence remains descriptive rather than fully causal.

Preprocessing dependence. The broad ordering is weaker under raw activations, layernorm-style normalization, and especially per-sample L2 normalization. The current findings are therefore strongest for the present z-score preprocessing protocol rather than for every reasonable preprocessing choice.

Category design. Our 16 categories are human-defined and may not align perfectly with the model's native structure. We partially address this with unsupervised SAE feature discovery, which finds category-selective structure without supervised category labels at feature construction time. However, interpretation is still anchored to the same evaluation taxonomy when we map features back to categories.

Four models. With only four models, cross-architecture correlations have limited statistical power. Extending to more architectures would strengthen generalization claims.

Intervention granularity. Our causal tests use linear direction ablations, which are informative but coarse. Stronger causal evidence would require token-level activation patching and generation-level behavioral readouts.

5 Related Work

Probing classifiers have been widely used to investigate linguistic properties in neural networks [Belinkov et al., 2017, Conneau et al., 2018, Hewitt and Manning, 2019]. Our work extends this to broader cognitive domains across multiple architectures.

Layer-wise analysis has revealed that lower layers encode syntactic information while higher layers encode semantic content [Jawahar et al., 2019, Tenney et al., 2019]. We find a similar early-to-late hierarchy but across 16 cognitive (rather than linguistic) categories.

Mechanistic interpretability approaches including sparse autoencoders [Cunningham et al., 2023, Bricken et al., 2023] provide complementary insights by identifying individual features rather than category-level representations.

Cross-model comparison has been explored through representational similarity analysis [Kriegeskorte et al., 2008] and model stitching [Bansal et al., 2021]. Our emergence correlation analysis contributes a new metric for comparing models at the level of cognitive development trajectories.

6 Conclusion

We have presented a layer-wise analysis of cognitive specialization in four LLM architectures, revealing broad early-to-late regularities, architecture-specific information dynamics, and systematic confusion patterns that reflect meaningful representational overlap. We also add SAE-based unsupervised feature discovery as a nonlinear validation layer, showing dense active feature inventories, strong category selectivity, and substantial cross-model feature alignment. The strongest supported claim is therefore a conservative one: broad category ordering survives several robustness checks, coarser taxonomies, and multiple control analyses, but exact timing remains architecture-sensitive, preprocessing-sensitive, and statistically underpowered at the current scale.

Future work. We plan to (1) build a true paraphrase replication set with fresh activations, (2) combine probing with sparse autoencoder feature discovery to bridge category-level and feature-level interpretability, and (3) strengthen causal analysis with token-level intervention and generation-time behavioral tests.

References

Yonatan Belinkov, Nadir Durrani, Fahim Dalvi, Hassan Sajjad, and James Glass. What do neural machine translation models learn about morphology? In *Proceedings of ACL*, 2017.

Alexis Conneau, German Kruszewski, Guillaume Lample, Loïc Barrault, and Marco Baroni. What you can cram into a single vector: Probing sentence embeddings for linguistic properties. In *Proceedings of ACL*, 2018.

John Hewitt and Christopher D. Manning. A structural probe for finding syntax in word representations. In *Proceedings of NAACL*, 2019.

Ganesh Jawahar, Benoît Sagot, and Djamé Seddah. What does BERT learn about the structure of language? In *Proceedings of ACL*, 2019.

Ian Tenney, Dipanjan Das, and Ellie Pavlick. BERT rediscovers the classical NLP pipeline. In *Proceedings of ACL*, 2019.

Hoagy Cunningham, Aidan Ewart, Logan Riggs, Robert Huben, and Lee Sharkey. Sparse autoencoders find highly interpretable features in language models. In *Proceedings of ICLR*, 2023.

Trenton Bricken, Adly Templeton, Joshua Batson, Brian Chen, Adam Jermyn, Tom Conerly, Nick Turner, Ced Anil, Carson Denison, Amanda Askell, Robert Lasenby, Yifan Wu, Shauna Kravec, Nicholas Schiefer, Tim Maxwell, Nicholas Joseph, Zac Hatfield-Dodds, Alex Tamkin, Karina Nguyen, Brayden McLean, Josiah E. Burke, Tristan Hume, Shan Carter, Tom Henighan, and Chris Olah. Towards monosemanticity: Decomposing language models with dictionary learning. *Transformer Circuits Thread*, 2023.

Nikolaus Kriegeskorte, Marieke Mur, and Peter Bandettini. Representational similarity analysis – connecting the branches of systems neuroscience. *Frontiers in Systems Neuroscience*, 2(4), 2008.

Yamini Bansal, Preetum Nakkiran, and Boaz Barak. Revisiting model stitching to compare neural representations. In *NeurIPS*, 2021.

A Full Competency Heatmaps

Full competency heatmaps for all four models are provided in Figure 1. Each cell (l, c) represents the probing accuracy for layer l on category c, with green indicating high accuracy and red indicating low accuracy.

B Per-Model Emergence Details

Table 6: Layer specialization summary per model.

Metric	**DeepSeek**	**Qwen**	**Llama**	**Mistral**
Mean specialization score	0.038	0.049	0.042	0.042
Most specialized layer	2	34	3	31
Critical info-gain layer	19 (70%)	7 (20%)	2 (6%)	1 (3%)
Initial entropy (bits)	2.376	1.979	2.257	2.241
Final entropy (bits)	2.472	2.343	1.850	2.317
Entropy change	+0.096	+0.364	−0.407	+0.076

C Bootstrap Confidence Intervals

Full bootstrap results (1000 resamples) for emergence layers per category are shown in Figure 6. All key findings (universal emergence hierarchy, early-phase dominance, late-layer divergence) remain robust under resampling.

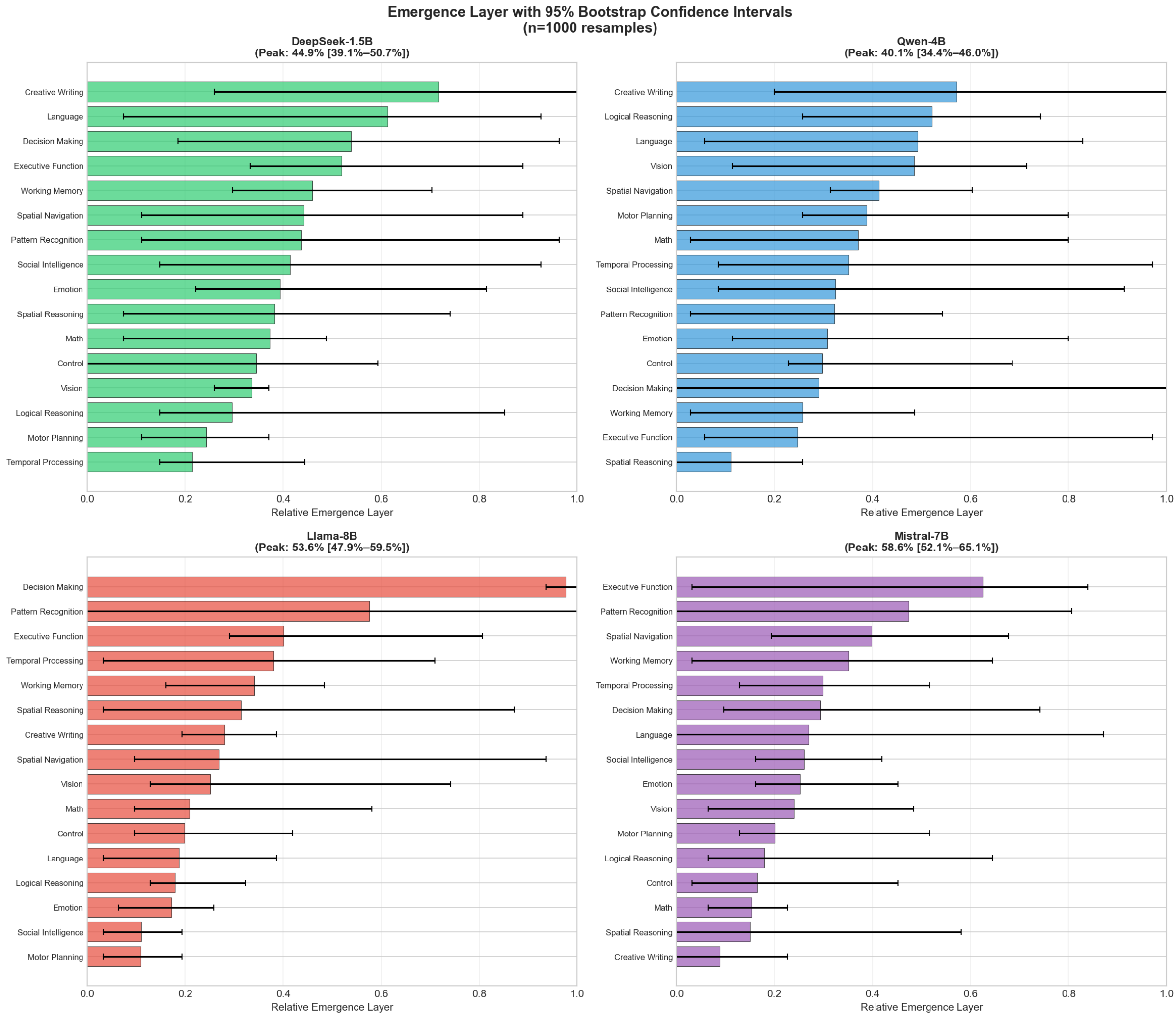

Figure 6: Bootstrap 95% confidence intervals for emergence layers; stability of emergence estimates.

D SAE Supplementary Diagnostics

This appendix extends Section 3.11 with additional diagnostics for feature inventory quality and training behavior. The same conclusions hold: feature dictionaries remain active, category-selective, and comparable across models.

The inventory view in Figure 7 is consistent with the main-text alignment analysis (Figure 5), providing an architectural comparison at the feature quality level in addition to category-selectivity structure.

Figure 7: SAE inventory diagnostics across models and expansion factors: active-feature counts, dead-feature fractions, and reconstruction quality.